Scientific Research Publishing

Open Journal of Civil Engineering, 2026, 16(1), 83-99
https://www.scirp.org/journal/ojce
ISSN Online: 2164-3172
ISSN Print: 2164-3164

# Application of *In-Situ* Live-Line Pole Replacement Technology in Iron Tower Construction

**Kongliang Chen[1*], Tao Zhang[2], Guoqing Yuan[1]**

[1]School of Civil and Architectural Engineering, Wuyi University, Jiangmen, China
[2]Jiangxi Applied Engineering Vocational Institute, Pingxiang, China
Email: *kongliangchen@126.com

**How to cite this paper:** Chen, K.L., Zhang, T. and Yuan, G.Q. (2026) Application of *In-Situ* Live-Line Pole Replacement Technology in Iron Tower Construction. *Open Journal of Civil Engineering*, **16**, 83-99.
https://doi.org/10.4236/ojce.2026.161005

**Received:** February 11, 2026
**Accepted:** March 10, 2026
**Published:** March 13, 2026



## Abstract

The transmission tower serves as a critical component of the national power transmission system, and together with overhead transmission lines, constitutes a nationwide power grid. However, as an indispensable part of transmission line infrastructure, it is highly susceptible to extreme structural failures such as overturning and collapse induced by external loads or material corrosion, which severely undermine the operational stability and safety of transmission lines. This paper proposes an innovative construction technique for replacing structural members of high-voltage transmission towers. The proposed method ensures the stability of the local member system during the replacement process and guides the construction under the coupled interaction of the tower-line system. A form-finding analysis of the ground wire is performed, deriving a mathematical model that characterizes the profile of transmission lines under combined self-weight and wind load conditions. By applying the equal-strength replacement principle and numerical simulation methods, the feasibility and practicality of *in-situ* live-line member replacement are verified. This method enables construction and maintenance work by replacing partial structural members without the need for complete tower dismantlement. Monitoring results indicate that the deformation deviations of the tower in all directions are maintained within the allowable safety range. Compared with conventional methods, this technique facilitates rapid *in-situ* live-line repair, offering remarkable advantages in terms of construction duration and economic efficiency.

## Keywords

Tower, Tower Line Shape, Numerical Analysis, Monitoring

## 1. Introduction

Over the past few decades, against the backdrop of rapid economic development, large-scale steel transmission tower projects have been constructed nationwide to satisfy the demands of infrastructure construction and expansion. However, transmission line towers are continuously exposed to harsh natural environments and must withstand extreme weather events as well as fluctuating structural loads, which gives rise to widespread corrosion and damage to key structural components such as tower bases. Thus, how to carry out efficient repair and reinforcement of tower structures has become a critical issue that cannot be overlooked. A comprehensive review of existing literature reveals that domestic scholars and practicing engineers have conducted a series of in-depth theoretical investigations and practical studies in this field, yielding fruitful results and accumulating valuable engineering experience [1]-[7].

Liu Xuewu *et al.* [8] studied the failure process, failure modes, and ultimate loads of reinforced transmission tower members and summarized the corresponding patterns. Chen Kongliang *et al.* [9] proposed an innovative low-cost technology is proposed to upgrade the foundation *in-situ* based on no power outages, and studied the analysis of the whole process of the *in-situ* live jacking construction. Furthermore, new progress has been made in research on tower reinforcement. Dinis *et al.* [10] used numerical analysis to investigate the global and local buckling behavior of equal-leg angle steel. Lu *et al.* [11] proposed a reinforcement method by attaching cross-shaped connecting elements outside the legs of the original angle steel to enhance capacity under increased wind and power loads. Oszvald *et al.* [12] investigated the buckling behavior of corroded equal-leg angle steel members through experiments. Research into the coupled behavior of transmission tower-line systems has gradually garnered attention. Wang Jia *et al.* [13] explored the dynamic coupling effect clarifying the performance mechanism of the tower-line system under various influencing factors. A new modeling method [14] for lattice transmission towers with retrofitted leg members was developed. Tapia *et al.* [15] used the pushover method to establish finite element models of two in-service transmission towers and conducted nonlinear buckling analysis under strong wind loads.

These studies have laid a solid theoretical foundation for addressing transmission tower-related issues. However, there have been few methodologies to prevent the collapse of severely corroded towers. Therefore, this paper comprehensively considers the local stability of tower structures and integrates a coupled tower-line system analysis. A numerical model of the transmission tower is established for both before and after member replacement scenarios, followed by an analysis of the support reactions under the most unfavorable wind direction and the stress distribution in the members to be replaced. The proposed method reduces construction costs and improves operational efficiency, and boosts construction efficiency substantially, whereas conventional reconstruction projects typically require around three months from design to completion, with at least three days of

forced power outage, and this method is mainly used for the member reinforcement of 110 kV and 220 kV transmission towers.

## 2. *In-Situ* Live Pole Change Plan of the Tower

### 2.1. Project Background

This research was conducted based on the practical engineering case of Tower #13 (shown in Table 1) on the Chengxiang Branch of the 110 kV Hantang Transmission Line, which is located in Fujian Province. The tower is situated within an orchard, with its foundation fully enclosed by the fruit-growing area. Due to the frequent application of herbicides and pesticides in the vicinity, long-term chemical residues, combined with rainwater and mist, have continuously dripped onto the tower components over time. This persistent exposure has kept the structural members and concrete surfaces in a prolonged damp state, ultimately leading to severe corrosion and even partial fracture of the tower structure, as shown in Figure 1.

Table 1. The parameters of tower #13.

| Transmission tower type | G-shaped | Transmission tower lines | 110 kV dual circuit | |
|---|---|---|---|---|
| Tower height | 40 m | Horizontal spacing | 270 m | |
| angle | 0˚ | The type of the base | Freestanding rigid foundation | |
| Wire model | | LGJ-900/75 | Calculated weight (N/m) | 30.086 |

Figure 1. Corrosion rods.

### 2.2. *In-Situ* Live Pole Replacement Method

Following comprehensive on-site inspections and investigations, relevant engineering and technical personnel proposed a member replacement method for high-voltage transmission towers. This approach leverages the tower's existing structural foundation to realize equal-strength replacement of corroded components.

The construction procedure of this method is described in this paragraph. Given the severe corrosion of the tower base members, temporary reinforcement was deemed a prerequisite construction step. Temporary supports were installed at the tower base, and the diagonal bracing on both sides of the main legs were reinforced by electric welding to preclude catastrophic failures such as tower overturning or collapse. After the temporary support system was securely established,

the corroded segments of the main legs were cut away. Drilling operations were then performed on both the original tower base and the residual intact angle steel. New angle steel members (16 Mn steel, L100×8 specification) were selected and connected by M20 high-strength bolts. These new angle steel members were externally fitted over the corroded main legs: their lower ends were bolted to the original tower base, while the upper ends were fastened to the existing main tower poles. Finally, all bolted connections were fully tightened and reinforced, as illustrated in Figure 2. During construction, the displacement of the tower base is controlled within 5 mm, ensuring the reliability of the operation through deformation monitoring.

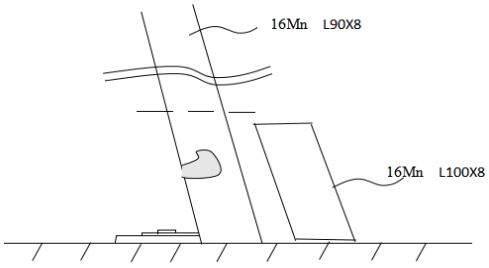


Figure 2. Temporary support schematic.

A supporting strut, fabricated from the same grade and size of angle steel as the main tower legs, was prepared with a length matching that of the removed corroded segment. This strut was installed in parallel with the existing structural members. Its lower end was welded to a dedicated connection base anchored to the concrete foundation, while the upper end was bolted to the externally fitted angle steel and fully secured, as illustrated in Figure 3. The joints between the new angle steel and the original tower components were further reinforced by electric welding. Upon completion of the main leg reinforcement work, the diagonal bracing on both sides were removed sequentially and replaced with new members of identical specifications.

Figure 3. Main pole replacement.

Upon finishing the replacement of all tower structural members, concrete was poured into the bearing supports of each temporary brace. The project was for-

mally completed after the cement achieved its designed strength following the required curing period. Following the above steps, treat the remaining three main poles and diagonal poles in the same way. After all the replacement and reinforcement are completed, spray paint to avoid corrosion at the joints, as shown in Figure 4.

**Figure 4.** The repair diagram of the tower.

## 3. Analysis of Tower-Line System

The overall transmission tower system is primarily composed of the tower structure and the conductor system, which operate synergistically as an integrated unit. The conductor system incorporates both power lines and ground wires. Given that wind loads, along with the self-weight of conductors and ground wires, exert a critical influence on the service performance of the tower-line system, the impact of the conductor system on structural behavior must be rigorously evaluated.

### 3.1. Checking Calculation of Member Stability

When structural members are subjected to axial loads alone or combined axial and lateral loads, eccentric tension or compression occurs if the line of action of the applied loads does not coincide with the centroidal axis of the members. This eccentricity further induces combined compression-tension and bending deformation. In this study, the stability performance of the transmission tower members under such combined compression-bending deformation was verified through rigorous checking calculations.

$$\frac{N}{\varphi \cdot m_N \cdot A} + \frac{M}{W \cdot \left(1 - 0.8 \dfrac{N}{\pi^2 EA / \left(1.1\lambda_x^2\right)}\right)} \le f \tag{1}$$

$$N_v^b = n_v \frac{\pi \cdot d^2}{4} f_v^b \qquad N_c^b = d \cdot \sum t \cdot f_c^b \tag{2}$$

The rod strength check calculation adopts formula (1), and $m_N = 1.0$, $\varphi = 0.9514$, $A = 15.64\ \text{cm}^2$, $I_x = 148.24\ \text{cm}^4$. The component can be regarded as a slender compression rod with one end fixed and one end hinged. Calculate

the shear bearing capacity $N_v^b$ and compressive bearing capacity $N_c^b$ of the bolt connection by formula (2).

In the formula [16]: $\lambda_x$ is the slenderness ratio of the component around the x-x axis; $N_{EX}$ is the parameter; $n_v$ is the number of shearing surfaces; $\sum t$ is the smaller total thickness of the pressure-bearing member in the same direction of force.

### 3.2. Conductor Geometry Analysis

The primary factors influencing conductor geometry include span length and sag. Prior to conducting geometric calculations, the fundamental assumptions for conductors must be satisfied. Given that conductors are flexible components incapable of withstanding compression or bending moments, they can be mechanically modeled as tension-only members, analogous to cables. Additionally, the load acting on the conductor is assumed to be uniformly distributed along its length. In this project case, the two adjacent transmission towers are assumed to be of equal height. Thus, the form-finding analysis of the transmission lines can be simplified to that of a catenary between supports at the same elevation. Within a typical span range, the configuration of the conductor between the two towers is depicted in Figure 5.

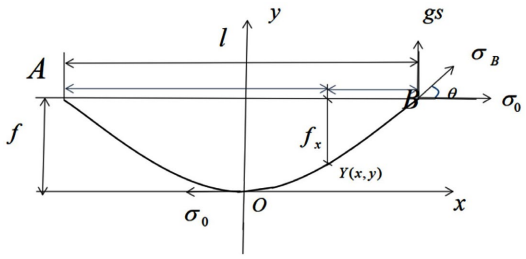


Figure 5. Catenary curve.

According to the above assumptions, the partial catenary element is taken for analysis, and the catenary equation of the wire in the working state can be derived as shown in Figure 6.

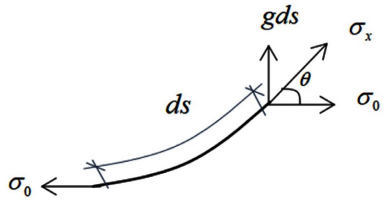


Figure 6. Catenary curve unit.

From the established functional relationship, we can derive:

$$\tan\theta = \frac{\mathrm{d}y}{\mathrm{d}x} = \frac{\sigma_g}{\sigma_0} = \frac{g\mathrm{d}s}{\sigma_0} = \frac{g}{\sigma_0}\sqrt{(\mathrm{d}x)^2 + (\mathrm{d}y)^2} \tag{3}$$

Differentiate Equation (3) to obtain the subsequent equation:

$$\mathrm{d}\left(\tan\theta\right)=\frac{g}{\sigma_0}\sqrt{1+\tan^2\theta}\,\mathrm{d}x \tag{4}$$

$$\frac{1}{\sqrt{1+\left(y'\right)^2}}\mathrm{d}y'=\frac{g}{\sigma_0}\mathrm{d}x \quad y'=\tan\theta \tag{5}$$

Integrate Equation (5) to obtain the subsequent equation:

$$arsh\frac{1}{y'}=\frac{g}{\sigma_0}x+c \tag{6}$$

$$y=\frac{\sigma_0}{g}ch\frac{g}{\sigma_0}\left(x+c_1\right)+c_2=\frac{\sigma_0}{g}\left(ch\frac{g}{\sigma_0}x-1\right) \tag{7}$$

$$f=y_1-y=\frac{\sigma_0}{g}\left(ch\frac{135g}{\sigma_0}-ch\frac{g}{\sigma_0}x\right) \tag{8}$$

In the formula: $g$ is the specific load of the overhead line; $\sigma_0$ is the axial stress at the lowest point of the overhead line; $S$ is the arc length of the selected unit; $f$ is the sag at any point of the overhead line and $x$ = 270/2 = 135 m, and the have Equation (8).

The catenary equation of the overhead line tower with equal height is derived, and the sag height at any point of the catenary is obtained when the span is 270 meters.

### 3.3. Static and Dynamic Analysis of Wind Load on Tower-Line System

Based on an extensive set of field-measured wind speed data, natural wind typically comprises two components: mean wind and fluctuating wind. Accordingly, the wind speed at any given height can be expressed as the sum of the mean wind speed and the fluctuating wind speed, and the total wind pressure can also be expressed as the sum of average wind pressure and fluctuating wind pressure.

$$v\left(z,t\right)=\overline{v}\left(z'\right)+v_f\left(z,t\right) \quad w=\overline{w}+w_f \tag{9}$$

Given that the logarithmic law delineates the idealized wind speed profile within the atmospheric boundary layer, this model is adopted herein to characterize the vertical distribution of mean wind speed, as expressed below.

$$\overline{v}\left(z'\right)=\frac{1}{k}\overline{v}^*\ln\left(\frac{z'}{z_0}\right) \tag{10}$$

And in this article, due to the small height of the iron tower, the pseudo-static action theory which simplifies the wind load to the static load on the iron tower is adopted. In this way, all wind loads imposed on the structure can be converted into static loads, thus simplifying the structure design and analysis. There are two common expressions of pseudo-static wind load. In this section, the average wind load wind-induced vibration coefficient amplification method is adopted, and the formula is as follows.

$$\overline{w}=w_0\beta_z\mu_s\mu_z \tag{11}$$

In the formula: $\mu_s$ and $\mu_z$ are the variation coefficient, $w_0$ is the basic wind pressure. Most countries have used this method.

In the analysis, since the turbulence integral scale of the Kaimal wind speed spectrum varies along the height, which can reflect the characteristics of the wind speed variation along the height of different tower positions, the Kaimal wind speed spectrum is used to simulate the wind speed time history. The expression is:

$$s_v(n) = 200u^2 \frac{x^2}{n(1+50x)^{5/3}} \tag{12}$$

In the formula: $x = nz/v_z$, $v_z$ is the average wind speed at $z$ height.

In addition, the time histories of fluctuating wind speeds at different spatial locations are not completely synchronized, and even uncorrelated. Therefore, the spatial correlation of fluctuating winds should be analyzed. For spatial problems, the spatial three-dimensional Davenport coherence function should be used to deal with:

$$Coh(n) = \exp\left[\frac{-2n\sqrt{c_x^2(x_i - x_j)^2 + c_y^2(y_i - y_j)^2 + c_z^2(z_i - z_j)^2}}{\overline{v}(z_i) + \overline{v}(z_j)}\right] \tag{13}$$

In the formula: $c_x$, $c_y$ and $c_z$ are the spatial attenuation coefficients in directions of *x*, *y*, and *z*.

In this section, we plan to use the autoregressive model (AR) of the linear filtering method to simulate the fluctuating wind speed. According to the principle of the AR model, the fluctuating wind speed time history of M relevant spatial points $[u(x,y,z,t)]$ can be expressed as:

$$[u(x,y,z,t)] = \sum_{k=1}^{p}[\psi_g][u(x,y,z,t-g\Delta t)] + [N(t)] \tag{14}$$

In the formula: $[\psi_g]$ is the order autoregressive coefficient matrix; $[N(t)]$ is the independent random vector matrix; $P$ is the order of the autoregressive model; $\Delta t$ is the time step.

For any point in space $i(i = 1,2,\cdots,N)$, the covariance of a random process $u_i(t), u_i(t-g\Delta t)$ with a time difference is:

$$\begin{aligned} R_{ui}(x,y,z,g\Delta t) = E\{u_i(x,y,z,t-g\Delta t) - E[u_i(x,y,z,t-g\Delta t)]\} \\ \cdot\{u_i(x,y,z,t) - E[u_i(x,y,z,t)]\} \end{aligned} \tag{15}$$

Since $u_i(x,y,z,t)$ and $u_i(x,y,z,t-g\Delta t)$ are stationary random processes with a mean value of 0, their covariance is the correlation function, and the value is a function of the time difference, which is:

$$R_{ui}(x,y,z,g\Delta t) = E[u_i(t-g\Delta t)u_i(t)] \tag{16}$$

Multiplying both sides of formula (16) by $[u_i(t-g\Delta t)] = [u_1(t-g\Delta t),\cdots,u_N(t-g\Delta t)]$ at the same time, and calculating

expectations on both sides at the same time, the relationship between correlation function matrix $[R]$ and autoregressive coefficient matrix $[\psi_g]$ can be obtained:

$$[R]=[\bar{R}][\psi_g] \tag{17}$$

Then multiply (14) by $[u(t)]=[u^1(t),\cdots,u^M(t)]$ at the same time, then we have:

$$[R_N]=[R_u(0)]-\sum_{g=1}^{p}[\psi_g]^{\mathrm{T}}[R_u(g\Delta t)] \tag{18}$$

Do Cholesky decomposition of $[R_N]$ to $[R_N]=[U][U]^{\mathrm{T}}$, and get the independent stochastic process vector matrix:

$$[N(t)]=[U][n(t)] \tag{19}$$

In the formula: $[n(t)]$ is a random number matrix that obeys the standard normal distribution.

After obtaining the autoregressive coefficient matrix and the random process vector matrix, Equation (14) is discretized according to the time difference, and finally the required pulsating wind speed time history vector expression is obtained:

$$\begin{bmatrix} u^1(i\Delta t) \\ \vdots \\ u^M(i\Delta t) \end{bmatrix}=\sum_{k=1}^{p}[\psi_g]\begin{bmatrix} u^1[(i-g)\Delta t] \\ \vdots \\ u^M[(i-g)\Delta t] \end{bmatrix}+\begin{bmatrix} N^1(i\Delta t) \\ \vdots \\ N^M(i\Delta t) \end{bmatrix} \tag{20}$$

In the formula: $i\Delta t=0,\cdots,T, g<i$; when $g>i$, assumes $u(t)=0$.

### 3.4. Wind Speed Time History Simulation

The wind speed time history mainly considers the average wind and pulsating wind. The average wind part is simulated according to the logarithmic law, and the pulsating wind is regarded as the wind that has experienced Gaussian random turbulence. In this section, the MATLAB R2018b programming program is mainly used for simulation, and the main parameters are shown in Table 2.

Table 2. Key parameters for time-history simulation of turbulent wind velocity.

| Parameter category | Value |
|---|---|
| Mean wind model | Law of logarithm |
| Pulsating wind model | Kaimal |
| Coherence function | Spatial three-dimensional Davenport coherence function |
| 10 m high average wind speed (m/s) | 20.7 |
| AR model order | 4 |
| Simulation duration (s) | 200 |
| Time interval (s) | 0.1 |

After numerical simulation, we can get the wind speed time history curve and wind speed auto power spectrum comparison curve at different heights according to the Kaimal pulsating wind speed power spectrum. Due to space limitations, some of the elevations can be listed, as shown in Figures 7-10.

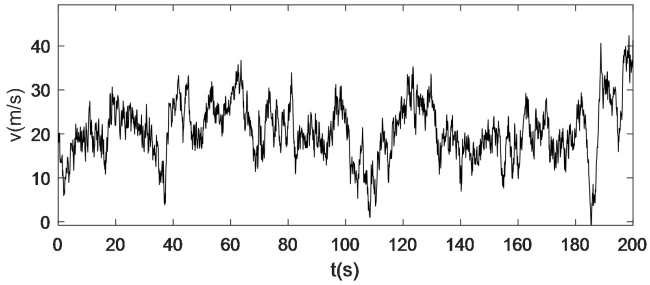


Figure 7. Z = 8 m height wind speed.

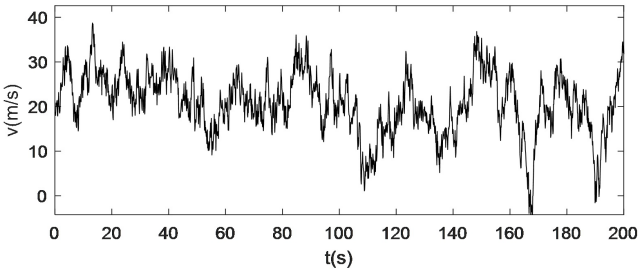


Figure 8. Z = 18 m height wind speed.

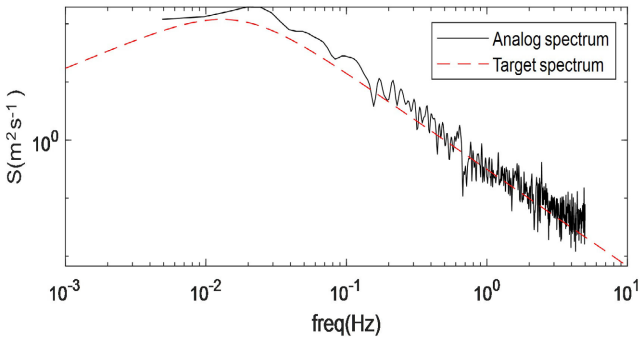


Figure 9. Comparison curve of self-power spectrum of 8 m wind speed.

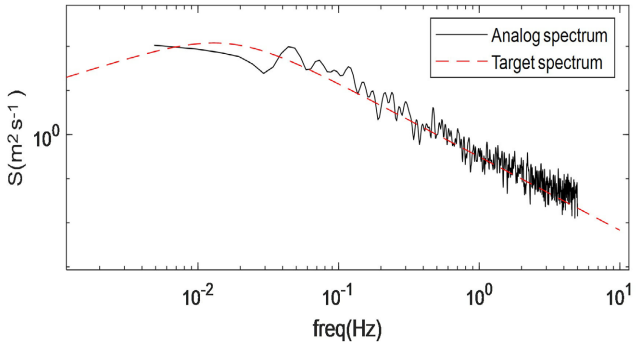


Figure 10. Comparison curve of self-power spectrum of 18 m wind speed.

In this study, the numerical simulation of fluctuating wind field is carried out using the Kaimal wind spectrum. The turbulence and spatial coherence parameters are set as: surface roughness length $z_0 = 0.05$ m, and Kaimal spatial coherence decay coefficients $c_x = 480$, $c_y = 360$, $c_z = 150$. The spatial measurement points are arranged along the height direction to accurately reproduce the turbulent structure of the atmospheric boundary layer near the ground.

The wind speed time history is generated by a 4th-order autoregressive (AR) model. The AR order is determined according to the attenuation characteristics of the wind speed autocorrelation function and the spectrum fitting accuracy. And the time step which shown in Table 2 satisfies the sampling theorem and high-frequency spectrum resolution requirements, ensuring stable and reliable simulation.

Based on the target Kaimal spectrum, in addition to intuitive comparisons in time and frequency domains, the coefficient of determination $R^2$ and relative error of spectrum integration are adopted to quantitatively evaluate the fitting performance. The results show that the coefficient of determination between the simulated spectrum and the target spectrum is $R^2 \geq 0.98$, and the relative error of spectrum integration is ≤5%, indicating that the two are highly consistent in both frequency-domain energy distribution and overall energy level.

## 4. Numerical Simulation Analysis

The primary consideration in establishing a tower-line coupling system for the transmission tower model is the selection of model elements. For the transmission tower's mechanical model, beam elements are adopted for analysis, while the transmission line's mechanical model is treated as a tension-only rod. Considering the safety and stability of the tower structure, Midas Civil is employed to model and analyze the stress state of the tower during the member replacement process, ensuring that the structural bearing capacity of the tower remains within the safety limits throughout the entire construction stage. The tower model is illustrated in Figure 11.

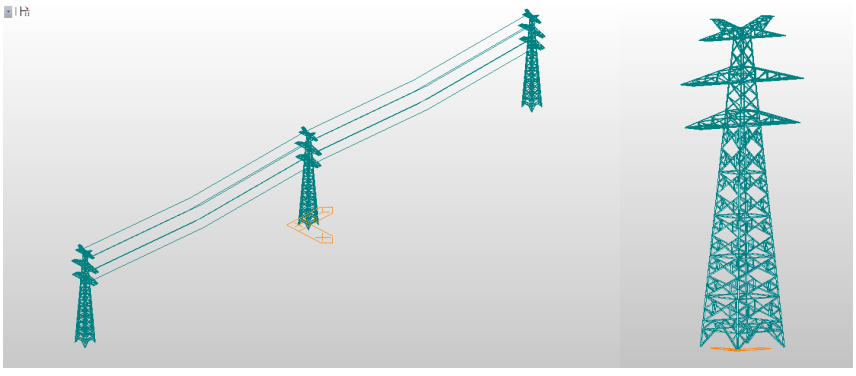

Figure 11. Tower-line system model.

The Midas Civil analysis process for the transmission tower is as follows. A fully fixed constraint is applied at the connection between the tower legs and the foundation to simulate the actual rigid restraint of the foundation on the tower body.

Structural members are modeled using beam elements, while the conductors are established using the aforementioned form-finding method. By specifying the initial tension, designed span length, and self-weight of the conductors, the system is allowed to reach its initial equilibrium state under gravity, corresponding to actual engineering conditions. Wind loads are primarily applied to the main body of the tower structure. For components such as the tower shaft and cross-arms, nodal wind loads are applied based on the conversion of the windward area.

In the process of pole change, the most unfavorable load combination of the tower under the action of wind load, wire-ground load and self-weight load of the tower is mainly considered. As shown in Figure 12 and Table 3, it is the vertical reaction force of the four supports A, B, C, and D when the iron tower is working normally. The largest support reaction force appears on the C support, which is 16.6 kN. The smallest bearing reaction force appears on the A bearing, and its magnitude is 12.9 kN. When the iron tower is working normally, the maximum stress among the four support towers A, B, C, and D is 4.9 MPa, and the minimum stress is 3.7 MPa, as shown in Figure 13.

Table 3. The reaction force of the front and rear supports of the tower.

| Support number | A | B | C | D |
|---|---|---|---|---|
| Normal working tower angle reaction force (kN) | 12.9 | 13.0 | 16.6 | 16.5 |
| Tower foot reaction force when replacing damaged members (kN) | 9.6 | 20.1 | 12.9 | 16.4 |

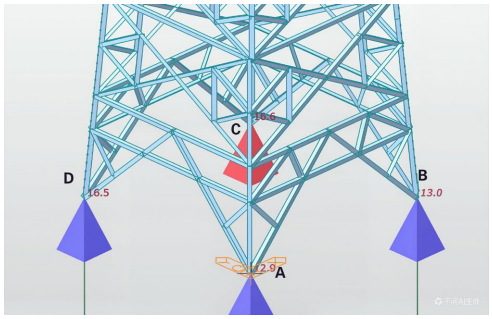


Figure 12. Normal working tower reaction force (kN).

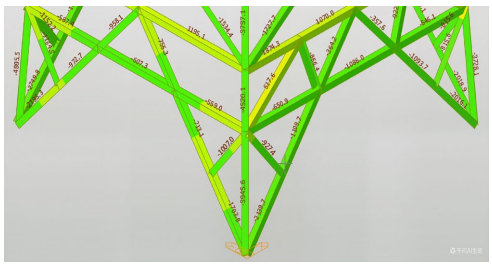

Figure 13. Normal working tower pole stress (kPa).

When the damaged component is removed and replaced with a new main pole, the most unfavorable wind condition must be taken into account. Specifically, the most adverse scenario occurs when the wind direction is perpendicular to the pole

being replaced, corresponding to a wind attack angle of 90˚. As shown in Table 2, the maximum support reaction of 20.1 kN occurs at Support C under this condition, while the reaction at this support drops to 9.6 kN after the damaged rod is removed. This indicates that the load originally borne by the damaged rod is primarily redistributed to Support C. Meanwhile, the removal of main pole leads to a significant increase in the stress of the web members on both sides of the tower respectively. Despite this notable stress elevation, the maximum compressive stress accounts less than one-tenth of the design strength, which is well below the ultimate bearing capacity limit state of the component. Thus, the tower structure remains safe throughout the construction process.

## 5. Monitoring Analysis

In order to further understand the lateral horizontal displacement of the apex of the tower and the vertical displacement of the four bases of the tower during the pole changing process, a unit was commissioned to monitor the horizontal and forward displacement of the reinforced tower.

### 5.1. The Condition of the Tower after Construction

After the pole replacement construction by the professional team, according to the monitored data, the maximum deviation of the tower in the cross-line direction of the tower is shown in Figure 14, and the maximum deviation of the tower along-line is shown in Figure 15.

As can be seen from Figure 14 and Figure 15, after the tower member replacement, the deflection values of the tower in both the along-line and cross-line directions are significantly reduced, indicating that the proposed high-voltage tower member replacement method can be effectively applied to the *in-situ* live-line repair of steel transmission towers.

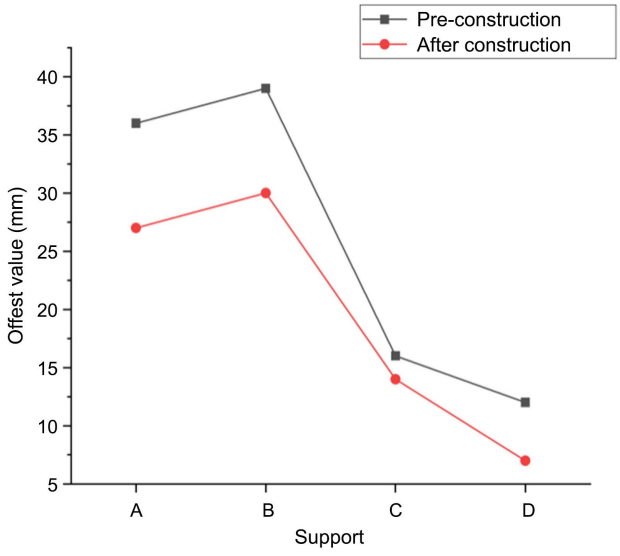


Figure 14. Cross-line deviation values.

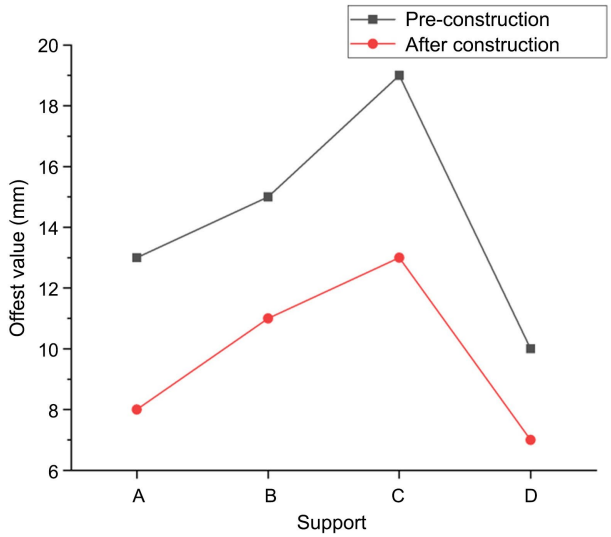


**Figure 15.** Along-line deviation values.

## 5.2. Application of *In-Situ* Live Pole Change Technology in Corner Tower

The preceding section discussed the application of *in-situ* live-line member replacement technology to tangent towers or towers with small tower-line turning angles in practical engineering. However, in actual scenarios, the steel towers that frequently require this operation are angle towers with large deflections, whose force transmission mechanisms may differ from those of tangent towers. Therefore, this section conducts a numerical simulation-based analysis of the *in-situ* live-line member replacement process for angle towers, and simulates the internal force variations of the angle tower's main members when the tower deflection angle ranges from 0˚ to 60˚. In addition, since the damaged members of the angle tower exhibit relatively low load-bearing capacity during the replacement operation within the 0˚ - 60˚ deflection range, climbing cables should be installed in the corresponding orientation of the tower to prevent structural tipping during construction. The internal forces exerted on the climbing cables throughout the *in-situ* live-line member replacement process also warrant analysis, and the numerical model established is presented below.

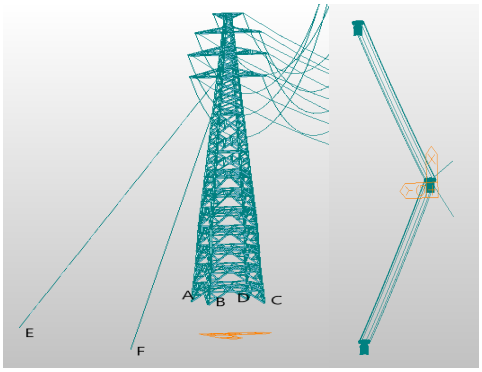


**Figure 16.** Schematic diagram of corner tower model.

As shown in Figure 16, the most unfavorable wind direction is along the positive direction of the y-axis, so line E and line F are set on both sides of them, and the reaction forces of tower supports at different corners are analyzed. The reaction force of the main pole support of the tower under the corner changes, as shown in following Table 4.

Table 4. Reaction force of iron tower support with different corners.

| Tower angle (degrees) | Support A reaction force (kN) | Support B reaction force (kN) | Support C reaction force (kN) | Support D reaction force (kN) |
|---|---|---|---|---|
| 0 | 12.8 | 13.1 | 16.5 | 16.4 |
| 10 | 11.6 | 12.1 | 17.3 | 16.9 |
| 20 | 11 | 11.3 | 18.1 | 17.5 |
| 30 | 9.6 | 9.8 | 18.9 | 18.2 |
| 40 | 8.9 | 9.2 | 19.3 | 18.8 |
| 50 | 8.2 | 8.7 | 19.8 | 19.2 |
| 60 | 7.8 | 8.2 | 20.3 | 19.7 |

It can be observed that as the inclination angle increases, the Z-direction axial forces of the four main poles of the tower exhibit distinct regular variations with the rise of the rotation angle. The reaction forces of main poles A and B on the climbing side of the tower fluctuate with the rotation angle, showing a trend of increase followed by decrease as the tower's inclination angle grows. In contrast, the reaction forces of main poles C and D on the non-climbing side rise continuously with the increasing inclination angle of the corner tower.

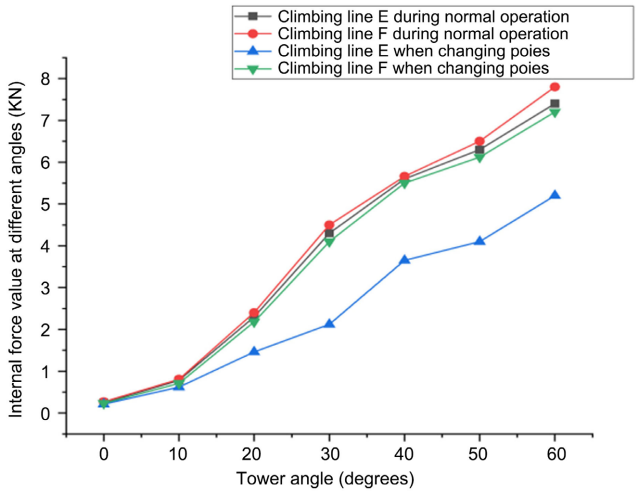


Figure 17. Internal force values at different angles before and after member replacement.

In addition, the internal forces and stresses of the climbing cables will gradually increase with the tilting of the corner tower as shown in Figure 17, yet their magnitudes are far below the allowable stress limits of the cables, indicating a state of

structural safety. It should be emphasized that when conducting *in-situ* live-line pole replacement on corner towers, the overturning effect induced by the eccentric tension forces from the overhead conductors and ground wires of the corner tower must be fully taken into account.

## 6. To Sum Up

The analysis results derived from the *in-situ* live-line pole replacement of the transmission tower are summarized as follows:

1) During the *in-situ* pole replacement operation, the tower structure is subjected to the most adverse loading condition at the stage where the damaged pole has been removed while the new pole is yet to be installed. At this critical juncture, a comprehensive verification was conducted on the compression-bending stability of the diagonal poles on both sides. Calculation results confirm that the bearing capacity of the bolts satisfies the design criteria after replacement. Following the completion of pole replacement, the main poles undertake the load-bearing function of the supporting section, thereby ensuring the overall structural stress state falls within a safe range.

2) Static and dynamic response analyses of the tower-line system, coupled with numerical simulation, reveal that the removal of a tower main pole will induce a significant stress surge in the web members on both sides. Nevertheless, the resultant stress values remain far below the material's allowable bearing stress, indicating that the tower is theoretically in a relatively safe condition during the *in-situ* pole replacement process.

3) A comparison of the tower displacement data monitored before and after the operation demonstrates that the *in-situ* live-line pole replacement effectively mitigates the tower's original abnormal inclination. This measure not only safeguards the tower's normal operational performance and eliminates potential equipment hazards, but also ensures the long-term structural health of the facility.

4) Based on the structural analysis of the steel tower and the innovative optimization of construction techniques, which has been validated for straight towers in previous studies and exhibits broad application prospects for corner towers as well. It holds groundbreaking significance for addressing structural safety hazards in transmission line towers.

## Funding

The paper is supported by the Special Funds of the National Natural Science Foundation of China (52408489).

## Conflicts of Interest

The authors declare no conflicts of interest regarding the publication of this paper.

## References

[1] Tang, Z., Han, C., Li, H., Fan, Z., Sun, K., Huang, Y., *et al.* (2024) Automatic 3D

Modeling Technique for Transmission Towers from 2D Drawings. *Mathematics*, **12**, Article 3767. https://doi.org/10.3390/math12233767

[2] Baran, E., Akis, T., Sen, G. and Draisawi, A. (2016) Experimental and Numerical Analysis of a Bolted Connection in Steel Transmission Towers. *Journal of Constructional Steel Research*, **121**, 253-260. https://doi.org/10.1016/j.jcsr.2016.02.009

[3] Bi, W., Tian, L., Li, C., Ma, Z. and Pan, H. (2023) Wind-Induced Failure Analysis of a Transmission Tower-Line System with Long-Term Measured Data and Orientation Effect. *Reliability Engineering & System Safety*, **229**, Article ID: 108875. https://doi.org/10.1016/j.ress.2022.108875

[4] Xu, Z., Zhang, T., Ge, X.D., Gao, F., Zhang, L.Y., Zhang, X. and Tian, L. (2021) Uncertainty Analysis of Transmission Tower-Line System under Wind Load. *Journal of Shandong University* (*Engineering Science Edition*), **51**, 1-7.

[5] Yang, X.J., Jinshan, M., Zhang, J.G. and Lei, Y. (2021) Effective Simulation of Random Pulsating Wind Field in Transmission Tower-Line System Based on Interpolation and Dimensionality Reduction Methods. *Vibration and Shock*, **40**, 77-83.

[6] Cao, M.G., Kuang, C.L., Wang, Y., He, C., Zheng, C. (2025) Mechanism and Wind Resistance Performance Assessment of Internal Cable Reinforcement for Transmission Tower under Extreme Winds. *Journal of Tsinghua University* (*Science and Technology*), 1-10. https://doi.org/10.16511/j.cnki.qhdxxb.2026.26.003.

[7] Liu, M.L., Lu, H.K., Luo, K., Wang, M.J., Fan, J.R. and Chi, W. (2020) Numerical Simulation of Wind-Induced Response of Transmission Tower-Line System under Real Mountain Terrain Conditions. *Vibration and Shock*, **39**, 232-239.

[8] Liu, X., Xia, K., Gao, Y., Liu, S. and Ren, X. (2011) Study on Strengthening the Structure and Its Design for the Transmission Tower. *Journal of Xi'an University of Architecture & Technology*, **43**, 838-844.

[9] Chen, K. and Shi, Y. (2023) *In-Situ* Live Jacking Technology of Corner Transmission Tower. *Sustainable Energy Technologies and Assessments*, **58**, Article ID: 103332. https://doi.org/10.1016/j.seta.2023.103332

[10] Dinis, P.B., Camotim, D. and Silvestre, N. (2012) On the Mechanics of Thin-Walled Angle Column Instability. *Thin-Walled Structures*, **52**, 80-89. https://doi.org/10.1016/j.tws.2011.12.007

[11] Lu, C., Ma, X. and Mills, J.E. (2018) Cyclic Performance of Bolted Cruciform and Splice Connectors in Retrofitted Transmission Tower Legs. *Thin-Walled Structures*, **122**, 264-285. https://doi.org/10.1016/j.tws.2017.10.020

[12] Oszvald, K., Tomka, P. and Dunai, L. (2016) The Remaining Load-Bearing Capacity of Corroded Steel Angle Compression Members. *Journal of Constructional Steel Research*, **120**, 188-198. https://doi.org/10.1016/j.jcsr.2016.01.003

[13] Wang, J., Fu, X. and Li, H.N. (2020) Multi-Factor Wind-Induced Dynamic Response Analysis of Transmission Tower-Line System. *Journal of Shenyang Jianzhu University* (*Natural Science Edition*), **36**, 1-10.

[14] Lu, C., Ma, X. and Mills, J.E. (2015) Modeling of Retrofitted Steel Transmission Towers. *Journal of Constructional Steel Research*, **112**, 138-154. https://doi.org/10.1016/j.jcsr.2015.04.005

[15] Tapia-Hernández, E., Ibarra-González, S. and De-León-Escobedo, D. (2016) Collapse Mechanisms of Power Towers under Wind Loading. *Structure and Infrastructure Engineering*, **13**, 766-782. https://doi.org/10.1080/15732479.2016.1190765

[16] Ministry of Housing and Urban-Rural Development of PRC (2017) Standard for Design of Steel Structures. GB 50017-2017, China Architecture & Building Press.